sciendo

ANNALS OF WEST UNIVERSITY OF TIMISOARA PHYSICS
Vol. LXVII, 2025

DOI: 10.2478/awutp-2025-0004

IMPACT OF RAPID THERMAL ANNEALING UNDER VARIOUS TEMPERATURES ON THE YTTRIUM OXIDE NANOPARTICLES

Alina Matei*[a], Oana Brîncoveanu, Cosmin Romaniţan, Cristina Pachiu, Vasilica Ţucureanu*[b]

National Institute for Research and Development in Microtechnologies (IMT-Bucharest), Erou Iancu Nicolae Street, 126A, 077190, Bucharest, Romania
**Corresponding author: e-mail: [a]alina.matei@imt.ro; [b]vasilica.tucureanu@imt.ro*

Article Info

Received: 13.08.2025
Accepted: 23.09.2025

Keywords:
Y_2O_3, chemical method, rapid termal annealing (RTA).

Abstract

In the present paper, the research was focused on the synthesis of Y_2O_3 nanoparticles (NPs) by a chemical method using yttrium nitrate hexahydrate, urea and ammonium hydroxide, deposition of the oxide precursors as thin films on silicon substrate, and drying in a desiccator at room temperature before thermal treatment. Then, the prepared samples were subjected to rapid thermal annealing (RTA) at a heating rate of 10 °C/sec. maintained at 600 and 900 °C for 600 sec., in nitrogen atmosphere. The morphological, structural, and wettability characteristics of Y_2O_3 films have been obtained using advanced analytical investigation tools. Morphological characterization (SEM) reveals nanometric particle sizes with a rough surface, and a slight tendency to agglomeration. The compositional analysis (EDX) revealed Y_2O_3 nanoparticles without impurities, supported by specific Y and O elements. The study of the vibrational characteristics of the synthesized samples was conducted using two complementary spectrometric techniques (FTIR and Raman), which revealed the characteristic vibration bands of the Y-O bond. The structural analysis (XRD) shows a cubic crystalline structure, revealing the high purity of the Y_2O_3 samples. The surface wetting capacity of Y_2O_3 films, as investigated by contact angle measurement, indicates a hydrophilic character and good percolation, with a direct impact on the performance of the material in various technological sectors.

1. Introduction

Oxide materials, particularly Y_2O_3, have proven very useful in advanced biomedical applications, with high impact in biosensors, biological imaging, photodynamic therapies, drug delivery systems, fluorescent biomarkers, bioactive ceramics, implants etc. Y_2O_3 NPs contribute to developing of efficient solutions in the targeted field due to their thermal stability, chemical durability, antioxidant and antibacterial activity, optical transparency, magnetic properties, and biocompatibility [1, 2].

Generally, Y_2O_3 is one of the most important rare-earth compounds, which exists in four structural phases, such as C-cubic (Ia3), B-monoclinic (C2/m), A-hexagonal (P32m) and H- hexagonal ($P6_3/mmc$ spatial group). It is known that, the cubic form is highly stable at ambient conditions, high temperature and normally preferred. It transforms to H-hexagonal phase at ~ 2400°C, respectively, to the B-monoclinic phase at ~10GPa. This type of oxide is a material with high refractory performance, good thermal conductivity, corrosion resistance, high up-conversion efficiency, great catalytic, activity, superior thermal and chemical stability. It also has excellent photoluminescence, optical and electrical properties. To obtain Y_2O_3 with established characteristics, the synthesis method and thermal treatment conditions are essential, having a strong impact on their physicochemical properties and performance [3-5].

In recent years, it has been proposed to synthesize Y_2O_3 nanoparticles by different chemical methods, which include sol-gel [6,7], hydrothermal [8,9], solution combustion [10], microwave solvothermal [11], co-precipitation [6,12,13], reverse microemulsion [14], thermal decomposition [15], spray pyrolysis [6,16], radio frequency thermal plasma methods [6,17], etc. Among them, precipitation is the most commonly used method to obtain Y_2O_3 NPs, due to the ease of process application, which features simple equipment, low cost, high yield, and economic reproducibility for large-scale production. By controlling the process parameters (concentration, reaction time and temperature, pH, and rate of addition of precipitation agents), as well as the appropriate thermal treatments, one can modify the size and shape of the particles, or the degree of purity [11, 13, 18].

In most cases, the thermal treatment applied to oxide materials, especially for Y_2O_3 is considered an important step with influence on morphological, structural, and optical characteristics. According to existing studies, thermal decomposition of precursors is achieved by conventional heat treatments using calcination furnace at relatively high temperatures and long time duration. Some of them have confirmed the impact of the temperature range 300-1100 °C, on microstructural, mechanical, optical, electrical properties, and extending the field of application by using Y_2O_3 thin films in semiconductor devices, dielectric for advanced electronic applications electrochemical sensors, etc [2, 12, 19-22].

In recent times, a special attention has been paid to rapid thermal annealing (RTA), as a result of its high temperature capability (maximum 1250 °C), high ramp rate and low dwell times, low energy consumption, use of inert atmosphere conditions (i.e. argon, nitrogen), controlled gas distribution, and controlled cooling down to ambient temperature. The carried-out research has revealed the possibility of using RTA treatments for the fabrication of oxide thin films (i.e. CuO, ZnO, ITO, CeO_2) at temperatures ranging from 300 to 1000 °C, in a time

range of the order of minutes, with effect on the functional properties of the synthesized materials [23-27].

In the present paper, we report the synthesis of Y_2O_3 nanoparticles by precipitation method, deposition of the oxide precursor as a thin film on silicon substrate, followed by RTA in nitrogen atmosphere at different temperatures (600°C and 900 °C) for 600 sec, with a ramp rate of 10 °C/sec. Also, the effect of RTA treatment on the morphological, structural, and wetting properties of Y_2O_3 films was investigated to extend the performance of the developed material.

2. Method and samples

2.1. Y_2O_3 nanoparticles synthesis

Synthesis of Y_2O_3 involves a typical precipitation process, using a soluble precursor containing yttrium [$Y(NO_3)_3 \cdot 6H_2O$, 0.05 M], urea [$CO(NH_2)_2$, 0.2 M] and ammonium hydroxyl [NH_4OH, 0.5 M] as precipitating agent, freshly prepared solutions.

In the first step, the required solutions of desired concentration were prepared by dissolving the Y^{2+} salt and precipitates in deionized water (DIW). A predetermined volume of urea was stirred together with DIW at a temperature above 80 °C. The $Y(NO_3)_3$ solution and the difference in volume of $CO(NH_2)_2$ were added simultaneously under continuous stirring to the obtained solution. After addition of the main components, stirring was continued, maintaining the same temperature, the pH of the solution being maintained at ~5. The use of urea is necessary because it decomposes slowly upon heating above 80°C, with a controlled supply of OH^- and CO_3^{2-} anions, which results in a uniform particle growth [2]. The ammonia solution was added dropwise until pH = 10, stirring was continued for 3h until an opalescent white solution was formed. The colloidal solution is left overnight for maturation and precipitation, after which the supernatant was removed by centrifugation and decantation.

The precipitate obtained was washed with DIW, and the centrifugation - decantation - washing steps were repeated until a neutral pH was obtained and the reaction by-products were removed.

2.2. Deposition as thin films on silicon substrates

To remove the surface contaminants, the silicon substrate was degreased in acetone and isopropyl alcohol (IPA), followed by a cleaning step in Piranha solution (H_2SO_4:H_2O_2), and to remove the native SiO_2 oxide and improve the wetting capacity, it was immersed in DIP solution (HF:H_2O), then washed thoroughly with DIW and dried with nitrogen gas flow. The

yttria precursor was deposited by “drop casting” as thin films on the surface of the silicon substrate, and dried in an oven at 100 °C for 2 h.

2.3. Rapid thermal annealing (RTA)

A rapid thermal processing furnace (RTP, AS-One 100, Annealsys, France), which can reach a maximum temperature of 1250°C, with a ramp rate of 0.1-200 °C/sec, in inert gas (nitrogen and argon). The coated silicon substrates' rapid treatment annealing (RTA) was carried out at 600 and 900 °C for 600 sec, with a ramp rate of 10 °C/sec, in a nitrogen atmosphere. The same oven cooling rate was maintained until the temperature reached 200 °C, followed by slow cooling to ambient temperature. The impact of the two temperatures used on Y_2O_3 thin films was characterized from morphological, structural, and wettability points of view.

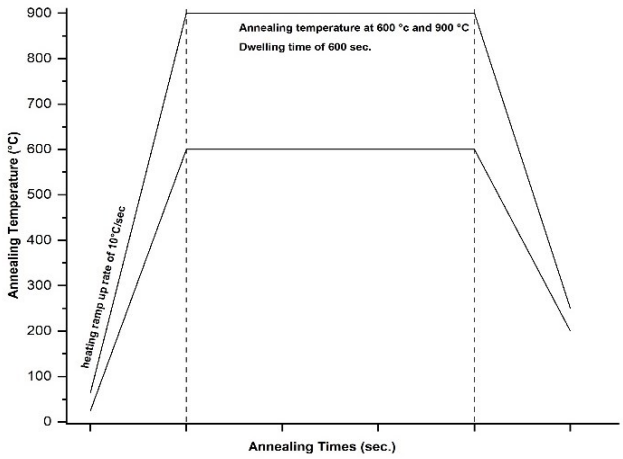

Figure 1. Diagram of RTA treatment and process conditions

2.4. Characterization

The surface morphological studies of synthesized samples were done using a Nova NanoSEM 630 Scanning Electron Microscope (FEI Company, Oregon, USA), with a Through-the-lens (TLD) detector at a magnification of 100kx, at an acceleration voltage of 10 kV. The compositional analysis was obtained using an Energy Dispersive X-Ray Analyzer (EDX) (Smart Insight AMETEK, Inc., Berwyn Pennsylvania, USA).

The chemical structure of the Y_2O_3 samples sintered RTA was studied using a Tensor 27 spectrometer (Bruker Optics, Ettlingen, Germany). Each sample was scanned by averaging 64 scans with a resolution of 4 cm^{-1} in the attenuated total reflection (ATR) mode using a Platinum holder. Raman spectra were collected using a Raman spectrometer (Alpha-

SNOM 300 S, WiTec. GmbH, Germany) under a visible (532 nm) laser excitation. The Raman spectra of yttrium oxide were taken under ambient conditions with the spectral acquisition time 20 s/scan, and data processing were performed on a dedicated computer using WiTec Project Five and Origin softwares.

The crystalline structure, crystallite size and purity of the samples were investigated by X-ray diffraction (XRD, Tokyo, Japan), using a Rigaku Smartlab with a Cu-K radiation source. This was operated at an operating voltage of 45 kV and a current of 100 mA supplied with CuKα radiation (λ = 1.5406 Å) in the 2θ range of 10–70°. The wettability capacity of Y_2O_3 films were performed using the Theta Optical Tensiometer (KSV Instruments) equipped with the CAM 101 camera and the 1394 firewire interface for fast image acquisition. The average of the measured contact angles was determined using Attension Theta software, using water with a volume varying between 2-2.5 µl.

3. Results and Discussions

3.1. Scanning electron microscope with energy dispersive X-ray spectroscopy (SEM-EDX)

Determination of morphological and compositional characteristics pf the synthesized samples were performed by SEM and EDX analysis. SEM micrographs and EDX spectra of Y_2O_3 samples obtained after RTA thermal treatment at different temperatures are presented in Figure 2. Surface analysis of Y_2O_3 nanoparticles reveals a uniform morphology with a rough surface, and very small particle size. According to the SEM image, increasing the treatment temperature from 600°C to 900°C, shows an up-sizing behavior of the particles and their tendency to agglomerate. This result could be justified by the process of nucleation and rapid growth in as short time at high temperatures with significant impact on the size, shape and agglomeration of the obtained particles [24].

EDX analysis confirmed that the Y_2O_3 nanoparticles were obtained without impurities, as evidenced by the assignment of energy maxima corresponding to specific elements in their composition, supported by the presence of yttrium (Y(L) at 1.92 keV) and oxygen (O(K) at 0.52keV) elements. Also, atomic and mass percentages corresponding to the elements (Y and O) are shown in the inset tables of the spectra, and close values were observed. The results indicate a Y/O ratio closely matches the theoretical stoichiometry of 2:3, as follows: $Y_{1.94}O_{3.06}$ for sample treated RTA at 600 °C, and $Y_{1.92}O_{3.08}$ for sample treated RTA at 900 °C.

The peak corresponding to the silicon (Si(K) at 1.739 keV) is characteristic of the substrate, and no other impurity peaks are identified.

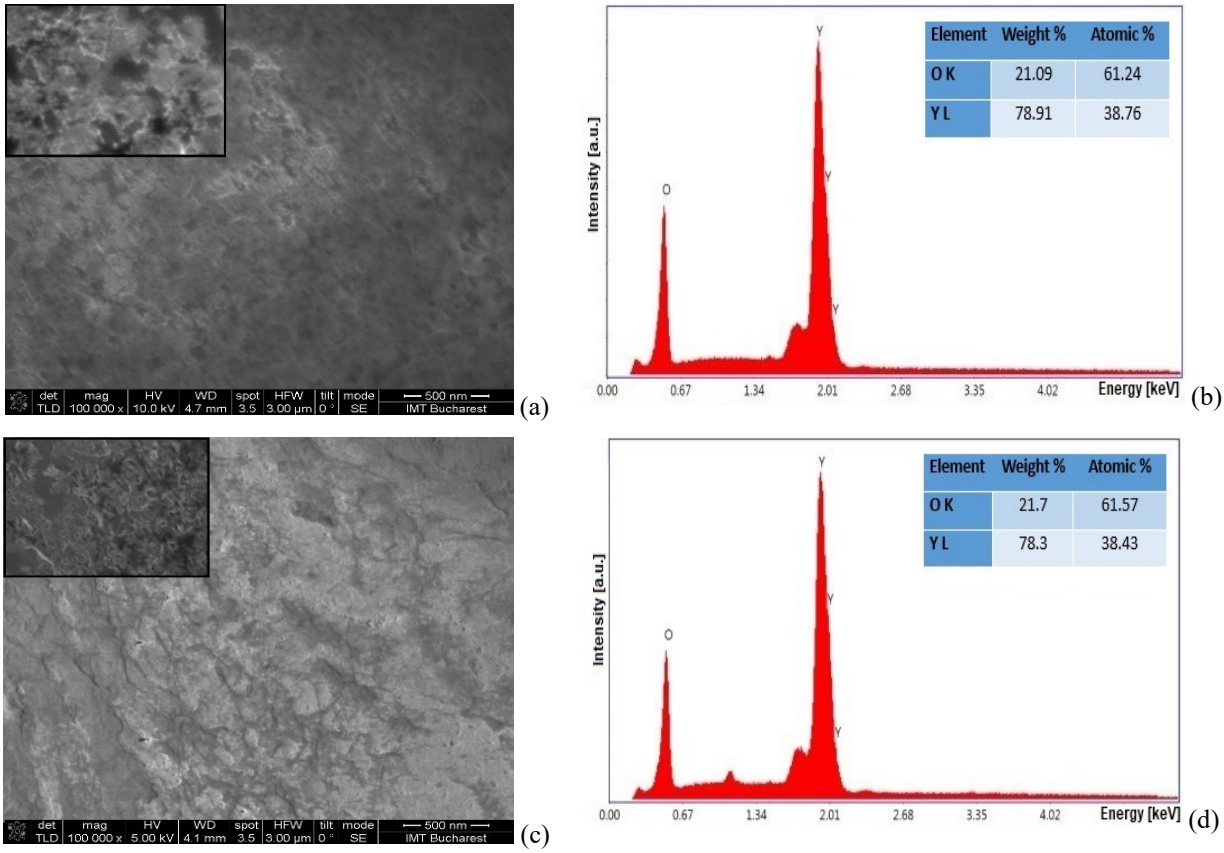

Figure 2. SEM micrographs and EXD spectra of the Y_2O_3 samples subjected to RTA treatment at 600 ˚C (a,b), and 900 ˚C (c, d)

3.2. Functional group analysis (FTIR)

FTIR spectroscopy was used to characterize the evolution of films subjected to RTA, in N_2 atmosphere. Figure 3 shows the FTIR spectra corresponding to the nitrate used as cation source and the oxide films subjected to thermal treatment at 600 and 900°C for 600 sec.

FTIR spectrum of yttrium(III) nitrate hexahydrate is mainly defined by the bands associated with the nitrate ion, but also with adsorbed water molecules. In the ranges 4000-3000 and 1700-1600 cm^{-1} specific bands are observed, which confirm the presence of water of crystallization. The other bands in the 1600-1000 cm^{-1} range are due to the stretching and deformation vibrations of the NO^{-3} group, and the maxima at 812, 749, 723 and 648 cm^{-1} show the interaction between the yttrium cation and the nitrogen anion [28, 29].

Given the short time applied to the RTA heat treatment, compared to a traditional thermal process at lower temperatures in air, it was necessary to increase the process

temperature, an observation confirmed by IR spectroscopy. In the spectra of the sample treated at 600 °C, low-intensity absorption bands can be observed, which may be associated with incomplete decomposition of the precursor. The bands in the spectral range 900-600 cm^{-1} can be attributed to the vibrations of the Y-O(H) clusters, which disappear at 900°C, due to total conversion to Y_2O_3 [30].

Absorption bands at 1516 and 1404 cm^{-1} are associated with the symmetric and asymmetric deformation vibration of the nitrogen ion, respectively, but the intensity of these bands decreases sharply with increasing process temperature. The X-ray diffraction data (see below) did not show the presence of nitrates, which may indicate the presence of traces of partially oxidized intermediates, without affecting the crystalline structure of the Y_2O_3 film. Also, in the spectrum of the sample treated at 600 °C, a maximum at 557 cm^{-1} associated with the vibrational mode of the Y-O bonds in Y_2O_3 can be observed. The bands observed in the spectrum of the sample treated at 900 °C at 558, 463, and 416 cm^{-1}, are specific to the stretching vibrations of the Y-O and Y-O-Y bonds in the yttria crystal structure, and become more intense with increasing temperature, which confirms the improvement in crystallinity [31-33].

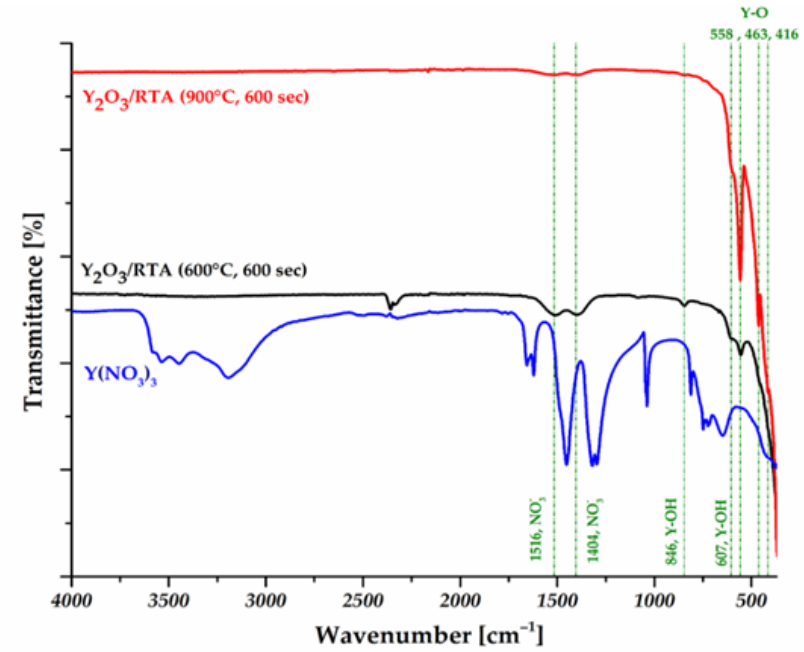

Figure 3. FTIR spectra for yttrium nitrate and oxide films subjected to RTA treatment at 600 ˚C, and 900 ˚C

3.3. Raman spectroscopy

Complementary studies to the FTIR spectroscopy were carried out by means of Raman spectroscopy to determine the chemical bonding and molecular structures of Y_2O_3 samples treated at different temperatures. The Raman spectra are presented in Figure 4, using

deconvolution of the Raman data by Gaussian fit. The spectra recorded for the two samples shows the peaks positions and symmetry of the identified peaks. For the samples treated at 600 °C, the presence of peaks centered at 135.3, 374.3 cm^{-1} that can be assigned to F_g mode, compared to those treated at 900°C where the peak at 528.5 cm^{-1} can be assigned to the F_g+E_g mode, characteristic of Y_2O_3 [34, 35].

No modes related to other phases or impurities have been detected, which is related to the fundamental vibrational mode of cubic Y_2O_3. Therefore, high temperature treatment improves the crystallinity of Y_2O_3, results which are in good agreement with XRD analysis.

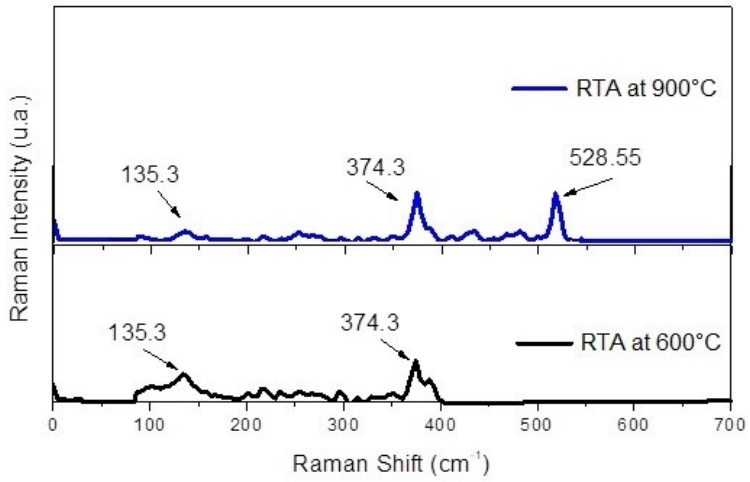

Figure 4. Raman spectra of the Y_2O_3 samples subjected to RTA treatment at 600 ˚C, and 900 ˚C

3.4. X-ray Diffraction

The structural and compositional characterization of the oxide films subjected to RTA treatment was performed by X-ray diffraction (XRD) measurements. From the XRD analysis presented in Figure 5, for the RTA synthesized samples at different temperatures, it can be observed the presence of Y_2O_3 with cubic structure (space group Ia3, 206), indexed according to the database.

The X-ray diffractograms of the synthesized Y_2O_3 samples indicate a high degree of crystallinity, with well-defined intensities of diffraction peaks observed at ~29°, 33°, 48°, and 57°, without other peaks characteristic, thus being confirmed the high purity of samples. For both samples a decrease of the contact angle was observed with increasing time, up to 21° after 30 sec. for the sample treated at 600 °C and up to ~ 43° for the sample treated at 900 °C, showing a good percolation capacity for both samples. Based on the Scherrer equation, the average size of the crystallites was calculated, indicating a value of 5.7 nm for samples treated at 600 °C, and with increasing temperature up to 900 °C, their size reaches 10 nm,

comparable with literature data. Studies have shown that as the size of the crystallites increases, with an effect on porosity reduction [36, 37].

The peak width at ~29° for the sample treated at 600 °C shows the existence of small crystallites, while the narrowing of the peak for the sample treated at 900 °C supports the increase in crystallite size.

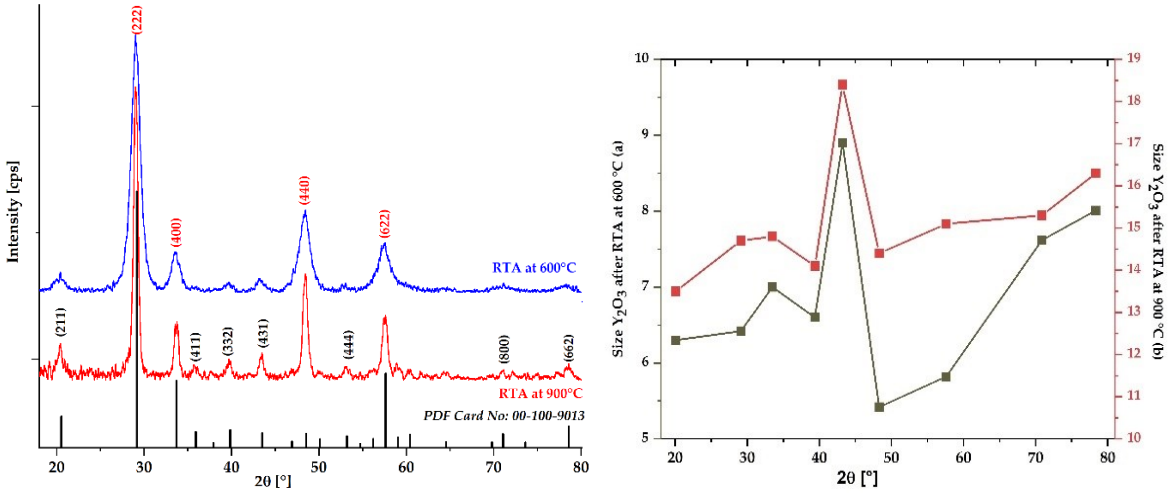

(a) (b)

Figure 5. XRD pattern (a) and crystallite size (b) of the Y_2O_3 samples subjected to RTA treatment at 600 ˚C, and 900 ˚C

The results of XRD analysis regarding the influence of the RTA temperature of Y_2O_3 on the average crystallite size, strain, lattice parameters, and atomic cell volume are presented in Table 1.

Table 1. Average crystallite size, strain, lattice parameters and atomic planes indexed with Miller indices.

Diffraction parameters	**Yttrium oxide (Y_2O_3)**		
	600°C	**900°C**	**Card No. 01-079-1716 / No. 01-100-9013**
Average crystallite size (nm)	5.7	10	-
Strain (%)	0.66	0.1	-
Lattice parameters			
a=b=c [Å]	10.649	10.645	10.606
Atomic cell volume [Å^3]	1207.61	1206.25	1193.04
Miller indices (hkl)	**2θ (°)**		
211	20.09	20.47	20.5
222	29.13	28.96	29.14
400	33.49	33.61	33.78
411	35.46	35.61	35.9
420	37.87	37.73	37.91
332	39.38	39.61	39.84
440	48.3	48.31	48.52
622	57.6	57.49	57.6

444	60.54	60.33	60.42
800	70.88	70.9	71.05
662	78.32	78.44	78.57

3.5. Wetting capacity (contact angle)

To determine the effect of the RTA treatment on the surface of Y_2O_3 films, measurements of contact angles and percolation capacity as a function of time are shown in Figure 6.

In general, the wetting degree is influenced by the surface properties (roughness, microstructure, etc.), and the type of liquid used. The surface hydrophilicity is evaluated by contact angles below 90°, and hydrophobicity by values greater than 90°, a behavior that varies with changing parameters. Measurements of the characteristic angles of Y_2O_3 samples in contact with water indicate a hydrophilic character, with values in the range $0 < \Theta < 90°$, depending on the applied temperature, surface morphology, and chemical composition of the films [35, 38, 39].

For the Y_2O_3 samples treated at 600 °C, a contact angle of 44° is observed, which indicates a good surface hydrophilicity. By increasing the temperature to 900 °C, the contact angle increases to 75°, keeping the same hydrophilic character, which confirms the influence of the RTA thermal treatment on the surface properties confirmed by SEM analysis. The percolation capacity of the Y_2O_3 films is evaluated by the variation of the contact angle with time, represented by the optical images presented in the graph. For both samples a decrease of the contact angle was observed with increasing time, up to 21° after 30 sec. for the sample treated at 600 °C and up to ~ 43° for the sample treated at 900 °C, showing a good percolation capacity for both samples.

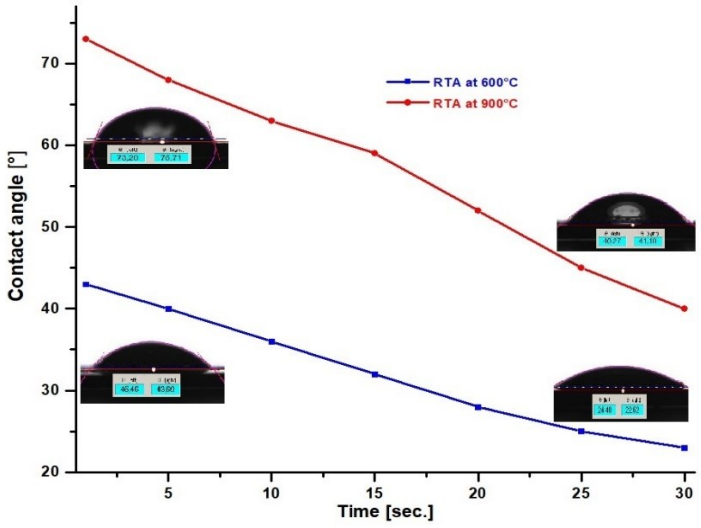

Figure 6. The contact angle of the Y_2O_3 samples RTA subjected to RTA treatment at 600 ˚C, and 900 ˚C

4. Conclusions

In summary, this paper reports the impact of rapid thermal annealing (RTA) on morphological, structural, and wettability characteristics of Y_2O_3. The influence of the RTA effect of precursor oxide films under different treatment conditions was studied, using the precipitation method and drop casting for deposition on silicon substrate, in order to synthesize yttrium oxide nanoparticles. By correlating the results, it is found that increasing temperature has an effect on morphological and structural properties.

The morphological analysis of the Y_2O_3 films indicates an increase in the agglomeration tendency, which is due to the rapid increase in temperature in a short period of time. Characterization of Y_2O_3 NPs by EDX analysis displaying the purity and chemical composition of the synthesized samples. The structural evolution of Y_2O_3 samples as a function of temperature shows that the temperature of 900 °C contributes to the increase in crystallite size and the variation of lattice parameters. The analysis of the wetting capacity of the water droplet on the surface of Y_2O_3 films shows an improvement of the percolation efficiency. The results show that the thermal treatment applied thin films to obtain Y_2O_3 nanoparticles improve the characteristics, which allows expanding their scope of applicability.

Acknowledgements

This work was supported by a grant of the Ministry of Research, Innovation and Digitization, CNCS-UEFISCDI, project number PN-IV-P2-2.1-TE-2023-0417 (BioYDetect, Contract no. 30TE/2025), within PNCDI IV.

References

[1] G. Rajakumar, L. Mao, T. Bao, W. Wen, S. Wang, T. Gomathi, N. Gnanasundaram, M. Rebezov, M.A. Shariati, I.-M. Chung, M. Thiruvengadam, Z. Zhang, Appl. Sci. 11 (2021) 2172

[2] T.M. Abdalkreem, H.C. Swart, R.E. Kroonr, Nano-Structures & Nano-Objects. 35 (2023) 101026

[3] R. Srinivasan, R. Yogamalar, A.C. Bose, Mater. Res. Bull. 45 (2010) 1165-1170.

[4] Y. Mao, J. Engels, A. Houben, M. Rasinski, J. Steffens, A. Terra, Ch. Linsmeier, J.W. Coenen, Nucl. Mater. Energy 10 (2017) 1-8

[5] L. Lia, S.A. Starostin, S. Li, S.A. Khan, V. Hessel, Chem. Eng. Sci. 178 (2018) 157–166

[6] Y.T. Foo, A.Z. Abdullah, B.A. Hori, B. Salamatinia, Ceram. Int. 44 (2018) 18693–18702

[7] R. Mellado-Vázquez, M. García-Hernández, A. López-Marure, P.Y. López-Camacho, A. de Jesús Morales-Ramírez, H.I. Beltrán-Conde, Materials 7 (2014) 6768-6778

[8] N. Li, K. Yanagisawa, J. Solid State Chem. 181 (2008) 1738– 1743

[9] G. Myvizhi, S.K. Krishna, Orient. J. Chem. 38 (2022) 312-317

[10] R. Ianos, R. Babuta, R. Lazau, Ceram. Int. 40 (2014) 2207–12211

[11] K. Chen, J. Peng, C. Srinivasakannan, S. Yin, S. Guo, L. Zhang, J. Alloys Compd. 742 (2018) 13-19

[12] S. Kumar, H. Tripathi, S. Bhardwaj, J.D. Sharma, U. Batra, IOP Conf. Ser.: Mater. Sci. Eng. 1033 (2021) 012049

[13] T. Saravanan, S.G. Raj, N.R.K. Chandar, R. Jayavel, J. Nanosci. Nanotechnol. 15 (2015) 4353–4357

[14] M.H. Lee, S.G. Oh, S.C. Yi, D.S. Seo, J.P. Hong, C.O. Kim, Y.K. Yoo, J.S. Yoo, J. Electrochem. Soc. 147 (2000) 3139-3142

[15] D. Tatar, H. Kaygusuz, F. tezcan, B. Erim, M.L. Ovecoglu, G. Ozen, NSTI-Nanotech (2008) 959-961

[16] X.L. Sun, A.I.Y. Tok, F.Y.C. Boey, C.L Gan, M.K. Schreyer, J. Mater. Res. 22(5) (2007) 1306-1313

[17] G. D. Dhamale, V. L. Mathe, S. V. Bhoraskar, S. N. Sahasrabudhe, S. Ghorui, J. Nanopart. Res. 17 (2015) 416

[18] S. Kumar, H. Tripathi, S. Bhardwaj, D. Garbiec, A Gupta, U. Batra, J.D. Sharma, J. Mol. Struct. 1302 (2024) 137463

[19] S. Thangabalu, N. Senthil kumar, T. Usha devi, S. Selvi, J.H. Chang, K. Mohanraj, Mater. Today Proc. 48 (2022) 229-233

[20] Y. Mao, J. Engels, A. Houben, M. Rasinski, J. Steffens, A. Terra, Ch. Linsmeier, J.W. Coenen, Nucl. Mater. Energy 10 (2017) 1–8

[21] R. Ivanic, V. Rehacek, I. Novotny, V. Breternitz, L. Spiess, Ch. Knedlik, V. Tvarozek, Vacuum 61 (2001) 229-234

[22] X.J. Wang, L.D. Zhang, J.P. Zhang, G. He, M. Liu, L.Q. Zhu, Mater. Lett. 62 (2008) 4235-4237

[23] P. Huang, H. Yang, Electronics 7 (2018) 213

[24] M.N.E. Boumezrag, K. Almi, S. Lakel, N.E.I. Zaghoum, H. Touhami, Annals of West University of Timisoara – Physics (2024) 76-94

[25] S. Dogar, S.D. Kim, Mat. Sci. Semicon. Proc. 56 (2016) 127–136

[26] P. Prepelita, I. Stavarache, D. craciun, F. Garoi, C. Negrila, B.G. Sbarcea, V. Craciun, Beilstein J. Nanotechnol. 10 (2019) 1511–1522

[27] Y. Guhel, T. Toloshniak, J. Bernard, A. Besq, R. Coq Germanicus, J. El Fallah, J.C. Pesant, P. Descamps, B. Boudart, Mat. Sci. Semicon. Proc. 30 (2016) 352–360

[28] J. L. Bishop, S. J. King, M. D. Lane, A. J. Brown, B. Lafuente, T. Hiroi, R. Roberts, G. A. Swayze, J.-F. Lin, M. Sánchez Román, ESS 8 (2021) e2021EA001844

[29] M.Y. Mihaylov, V.R. Zdravkova, E.Z. Ivanova, H.A. Aleksandrov, P.St. Petkov, G.N. Vayssilov, K.I. Hadjiivanov, J. Catal. 394 (2021) 245-258

[30] V. Tucureanu, C. Romanitan, I.A. Tudor, C. Tucureanu, M.A. Popescu, A. Matei, Ceram. Int. 46 (2020) 23802-23812

[31] X. Li, X. Liu, J. Qian, T. Zhang, B. Sun, Y. Han, Ceram. Int. 50 (2024) 27995-28003

[32] V. Tucureanu, A. Matei, A.M. Avram, Opto-Electron. Rev. 23 (2015) 239–251

[33] S. Kumar, H. Tripathi, S. Bhardwaj, D. Garbiec, A. Gupta, U. Batra, J.D. Sharma, J. Mol Struct. 1302 (2024) 137463

[34] J. Zhu, Y. Zhu, W. Shen, Y. Wang, J. Han, G. Tian, P. Lei, B. Dai, Thin Solid Films 519 (2011) 4894-4898

[35] H.C. Barshilia, A. Chaudhary, P. Kumar, N.T. Manikandanath, Nanomaterials 2 (2012) 65-78

[36] M. Hajizadeh-Oghaz, R.S. Razavi, M. Bareka, M. Naderi, S. Malekzadeh, M. Rezazadeh, J. Sol-Gel Sci. Technol. 78 (2016) 682–691

[37] J. Chen, B. Huang, C. Huamg, X. Sun, J. Rare Earths 35 (2017) 79-84

[38] A. Matei, M. Stoian, O. Brincoveanu, V. Tucureanu, Ceram. Int. 49 (2023) 19829–19839

[39] J.W. Song, L.-W. Fan, Adv. Colloid Interface Sci. 288 (2021) 102339